Supplementary Material

Direct preparation of PEA_2PbBr_4 nanoplates with electron-irradiation-induced optical evolution

Mingqun Zhang, Weili Liu, Jing Li, Shuai Yang, Hongwei Liang, Jiao Xu*, Yiming Yang

School of Integrated Circuits, Dalian University of Technology, No.321 Tuqiang street, Dalian 116024, China

* Author to whom correspondence should be addressed: xujiao@dlut.edu.cn

Experimental Section

Materials: $PbBr_2$ (>99.999%) was purchased from Sigma-Aldrich. Phenethylammonium bromide (PEABr) and n-butylammonium iodide (BAI) were purchased from Greatcell Solar Materials. N,N-dimethylformamide (DMF) and hydrobromic acid (HBr, 48 wt.% in H_2O) were purchased from Adamas-beta®. For operational safety, HBr was used after double dilution. All materials were used as received without further purification.

Material synthesis

1) Hydrobromic acid solution method

0.02 mmol $PbBr_2$ and 0.04 mmol PEABr are dissolved in a glass vial with 0.3 mL HBr. The perovskite mixed solution was heated on a heating plate at 120 °C under continuous magnetic stirring until the precursors were completely dissolved. Then the temperature was decreased to 38 ℃. 5 μL of the precursor solution was dropped onto a clean 1.5 cm×1.5 cm FTO glass substrate. The droplet was then covered with another 1 cm×1 cm FTO for spatial confinement growth.

2) Organic solution method

0.05 mmol $PbBr_2$ and 0.1 mmol PEABr are dissolved in a glass vial with 0.5 mL DMF. The perovskite mixed solution was continuously stirred until the precursors were completely dissolved. Subsequently, the same procedure described in 1) above was employed. The experimental setup was placed in a quiet, room-temperature environment to allow crystal growth. The growth process typically lasted for 1-3 days.

Gas-phase anion exchange

The substrate containing PEA_2PbBr_4 single-crystals was placed in a sealed glass vial. The iodide source of 20 mg BAI powder was evenly distributed at the bottom of the vial. Subsequently, the vial was placed on a hot plate with temperature of 170 °C for 30 minutes. The whole experiment was carried out in atmosphere.

Optoelectronic performance

Responsivity (R) and detectivity (D*) can be calculated by:

$$R = \frac{I_{light} - I_{dark}}{P \times S}$$

$$D^* = R\sqrt{S/(2eI_{dark})}$$

where I_{light} is the current under light illumination, I_{dark} is the current under dark

condition, P is laser power density and S is the effective area of the detector.

Material Characterization

In this study, photoluminescence (PL) spectra, optical microscope images and PL images were acquired using an Olympus BX53F microscope coupled with a spectrometer (Ocean Optics) and CCD camera (Olympus DP74). Both the magnetic heating stirrer (MS-H380-Pro) and the pipette were supplied by DLAB Dalong Instruments. X-ray diffraction (XRD) patterns were obtained using a SmartLab 9 kW diffractometer (Rigaku, Japan) with Cu-Kα radiation. Current-voltage (*I-V*) characteristics were measured using a high-precision source meter (Keithley 2450). The morphology and elemental composition of the samples were characterized using a scanning electron microscope (SEM, TESCAN MAGNA) equipped with an energy-dispersive X-ray spectroscopy (EDS) system (30 keV, 1 nA).

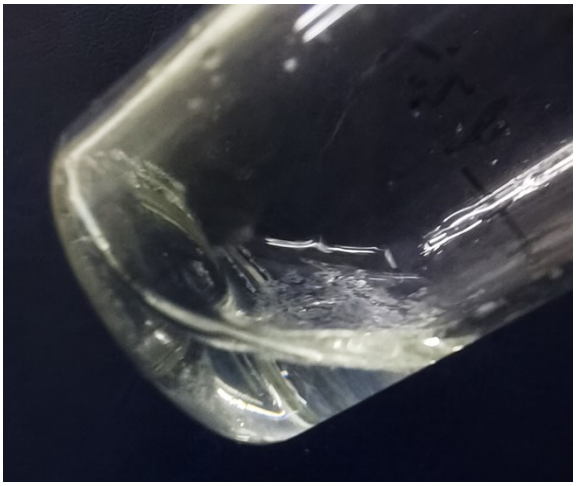

Fig. S1. The HBr-based PEA_2PbBr_4 precursor solution after cooling to room temperature.

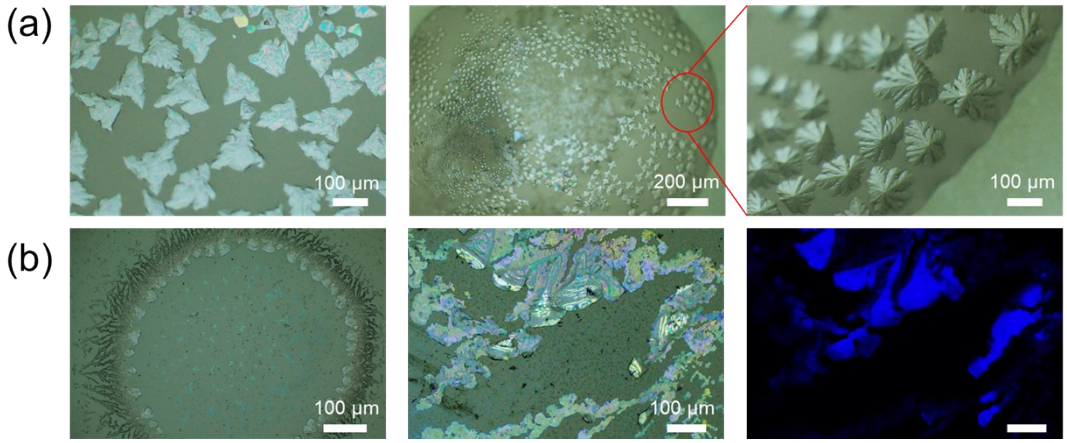

Fig. S2. (a) Dendritic crystals precipitated from the precursor solution at elevated T_{sat}. (b) Irregular crystals precipitated from the precursor solution maintained at room temperature.

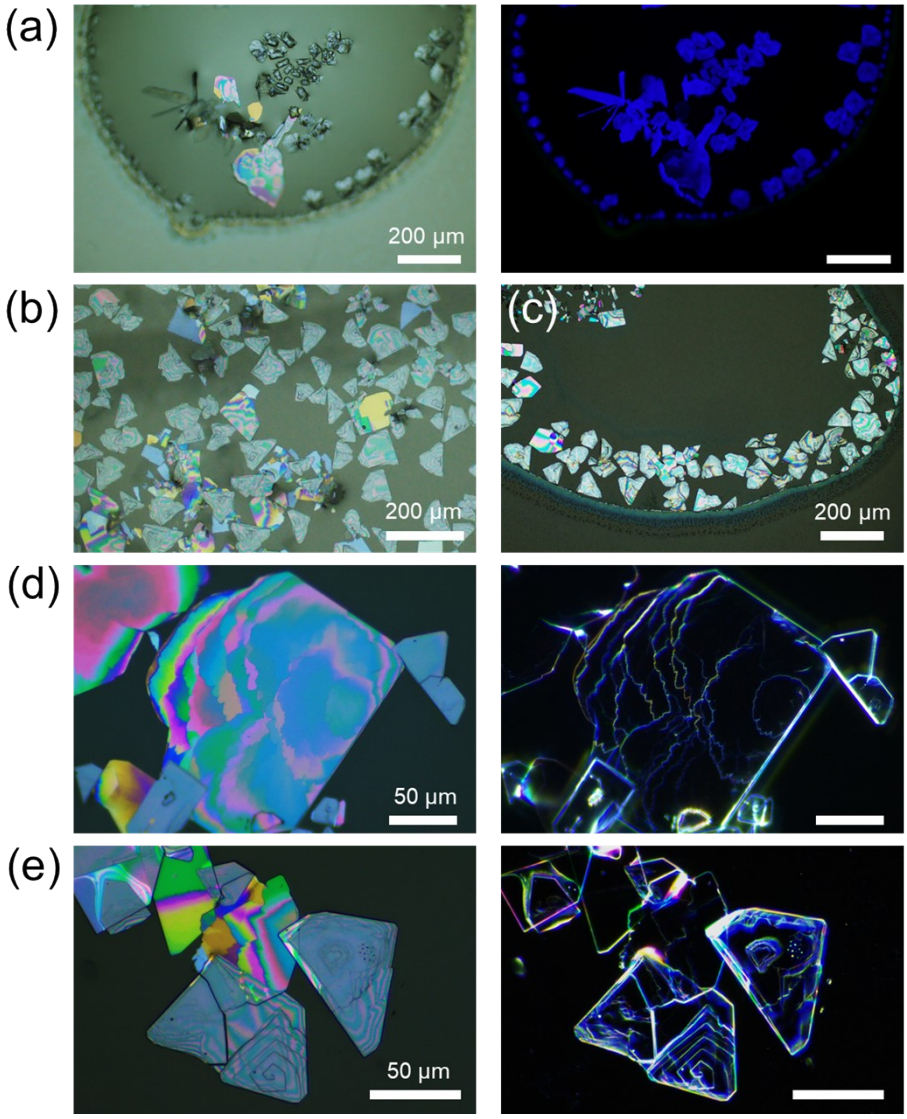

Fig. S3. PEA_2PbBr_4 crystals image via direct growth at 38 ℃. (a) OM and corresponding PL images of a small droplet. (b) OM image of a large droplet. (c) OM image after the droplet has evaporated. (d) Bright-filed and dark-field OM image of an irregular layered microplate. (e) Bright-filed and dark-field OM image of the microplate with spiral growth trace.

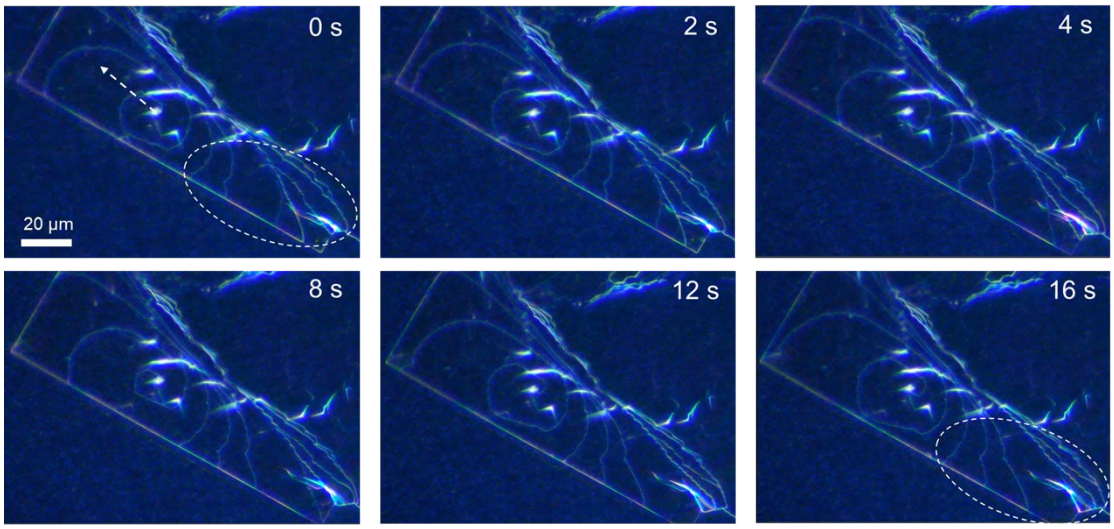

Fig. S4. Dark-field images captured at different growth time of a PEA_2PbBr_4 microplate prepared via direct growth method. Due to the continuous supply of solute in the solution, crystal growth proceeds through persistent layered diffusion from the center towards the edge. Arrows and ellipses indicate the points of change.

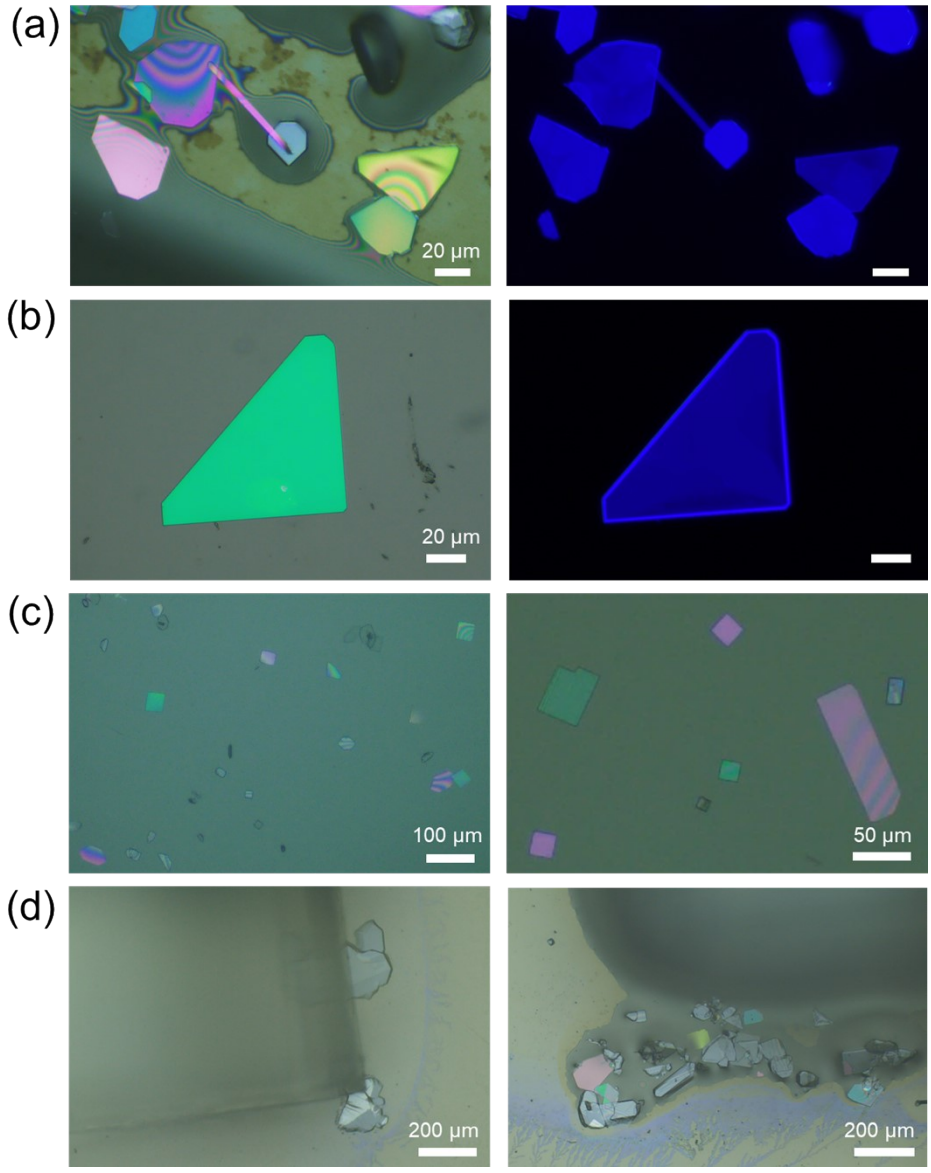

Fig. S5. OM images of PEA_2PbBr_4 nanoplates obtained via the spatial confinement method. (a, b) OM and corresponding PL images at the edge region. (c) OM image within the confined domain. (d) OM image of the edge region under excessive droplet condition.

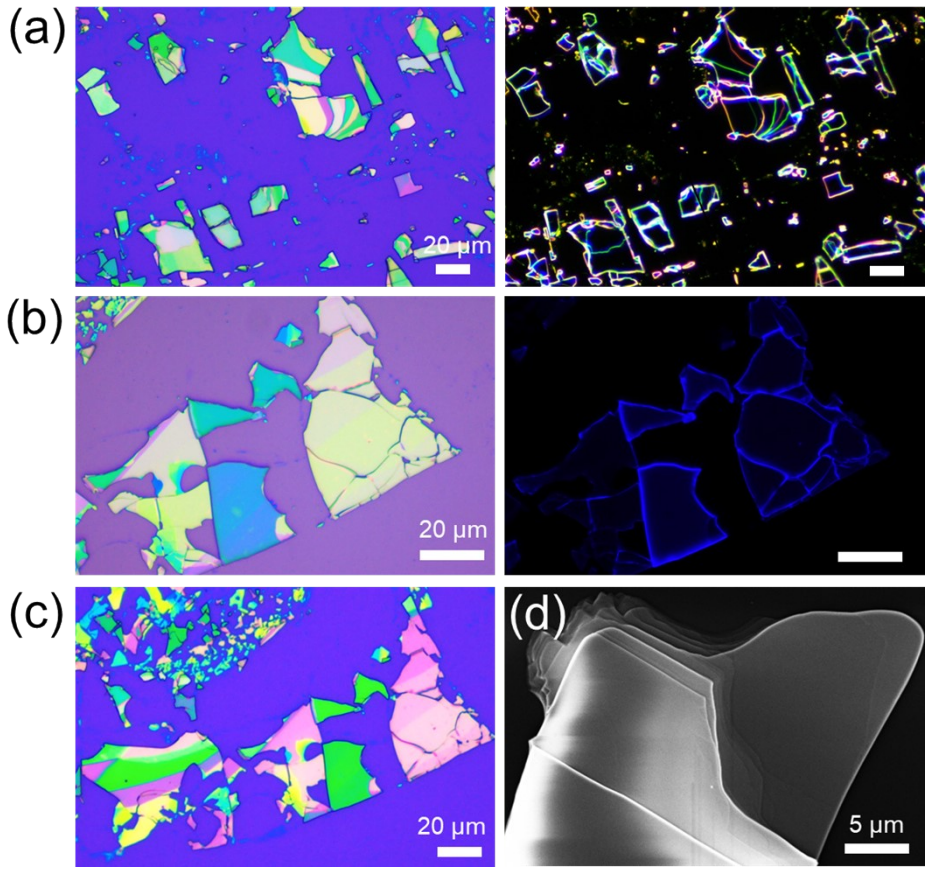

Fig. S6. Mechanically exfoliated PEA_2PbBr_4 by scotch tape. (a) Bright-field and dark-field images of exfoliated PEA_2PbBr_4 nanoplates. (b) OM and corresponding PL images of exfoliated PEA_2PbBr_4 nanoplates. (c) OM image of irregular nanoplates. (d) SEM image of a layered crystal.

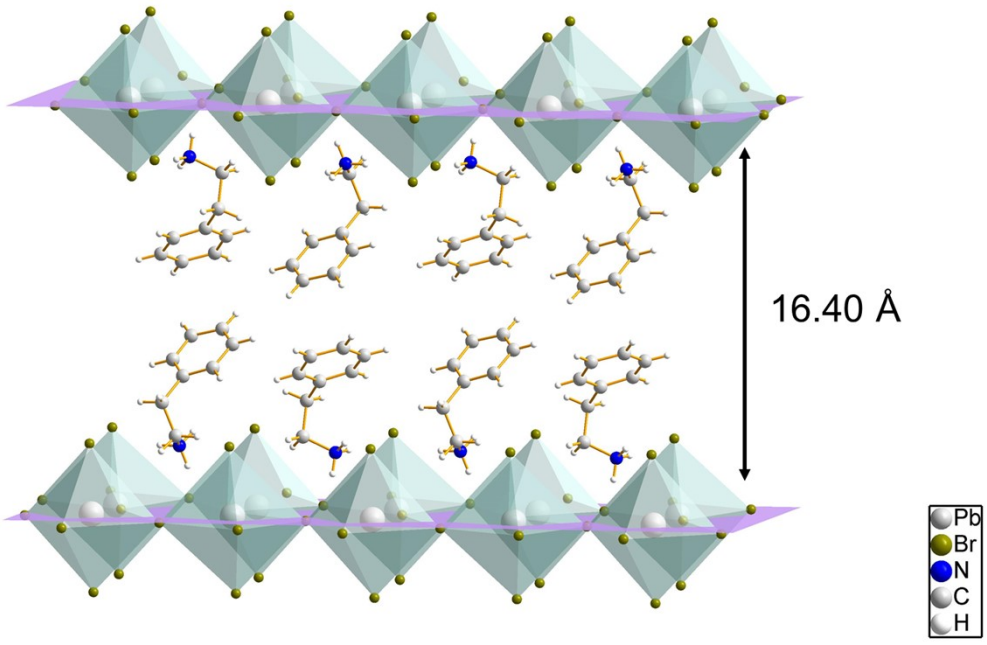

Fig. S7. The structure model of PEA_2PbBr_4 crystal.

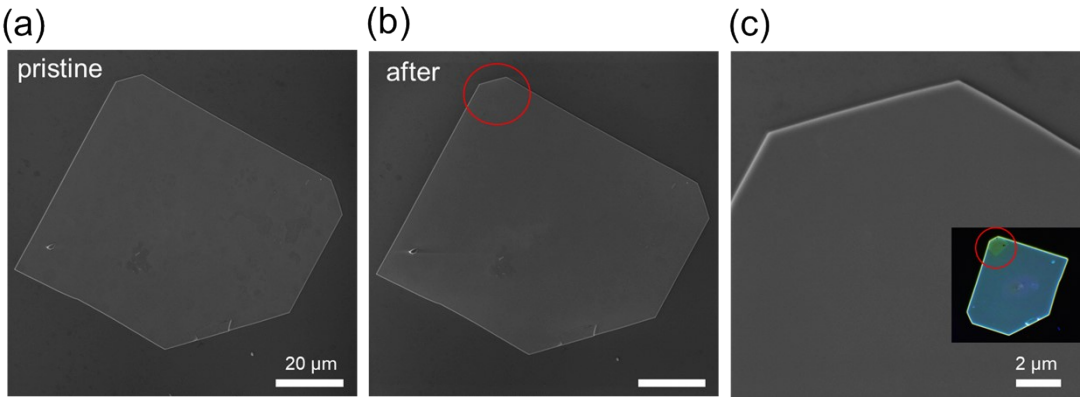

Fig. S8. SEM image of the PEA_2PbBr_4 nanoplate before (a) and after EDS (b), respectively. (c) Local SEM image after EDS. The inset is corresponding PL image the PEA_2PbBr_4 nanoplate. The red circle shows where the localized irradiation is located.

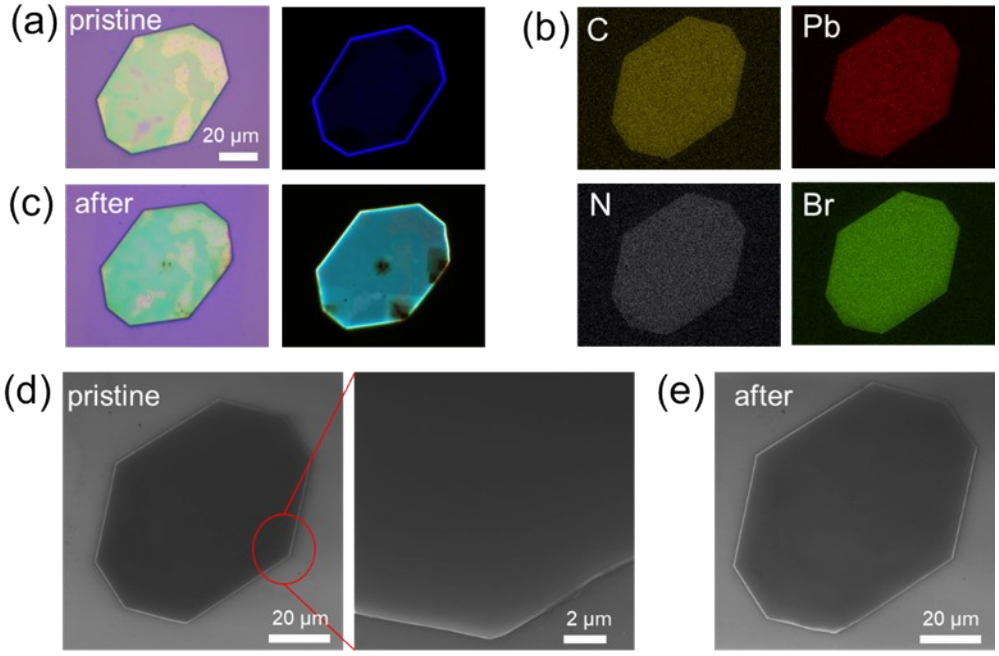

Fig. S9. (a) OM and corresponding PL image before SEM-EDS. (b) Elemental distribution map of the nanoplate. (c) OM and corresponding PL image after SEM-EDS. In particular, the blackening of crystal edges is caused by localized focusing under the high voltage of the SEM. (d) SEM image of the crystal and local enlargements before EDS. (e) SEM image after EDS.

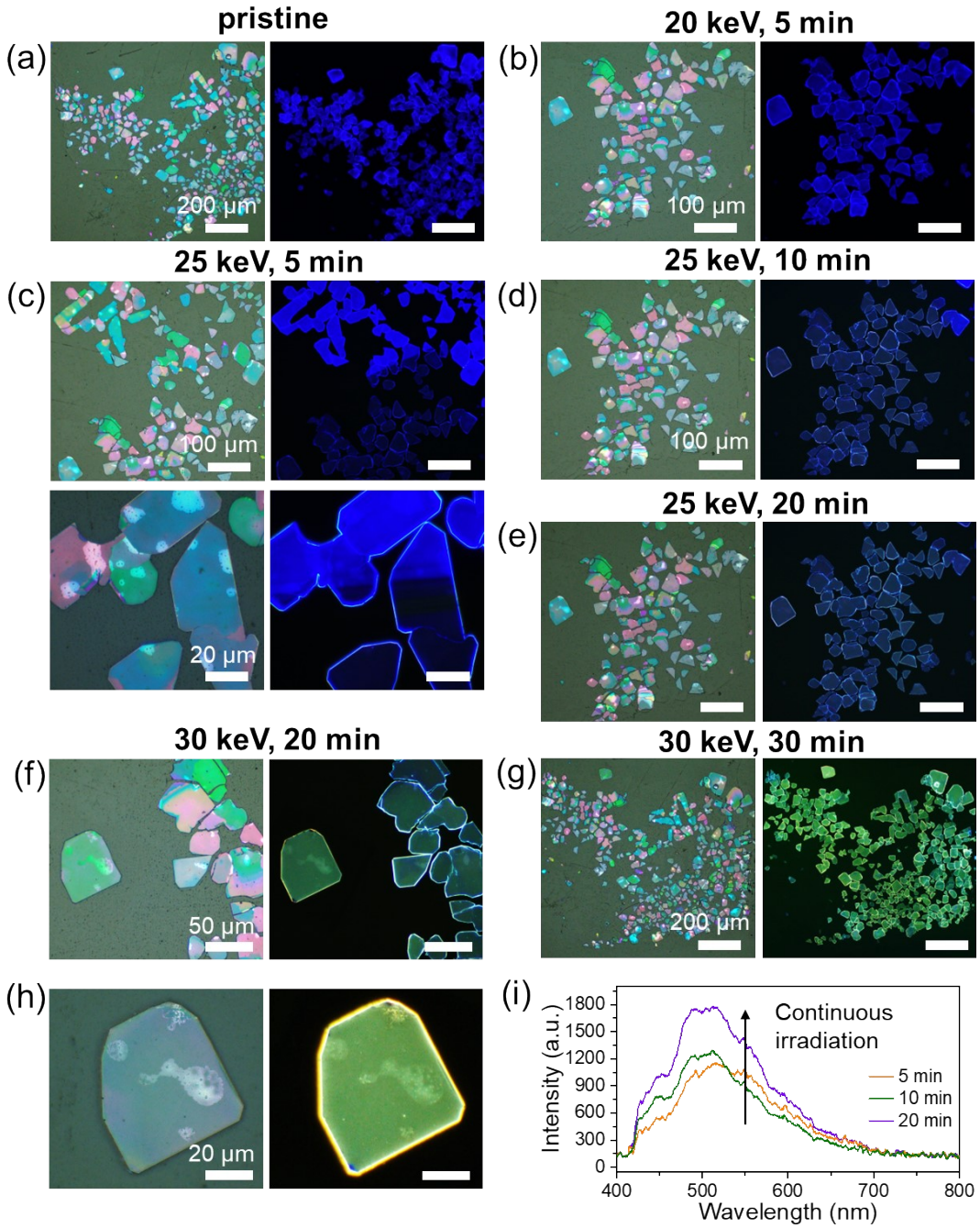

Fig. S10. OM and corresponding PL images of PEA_2PbBr_4 nanoplates under varying SEM accelerating voltages and irradiation durations. (a) Pristine sample. (b) 20 keV for 5 min. (c) 25 keV for 5 min. Local magnification (bottom panels) reveals a distinct light-dark interface. (d) 25 keV for 10 min. (e) 25 keV for 20 min. (f) 30 keV for 20 min. (g) 30 keV for 30 min. (h) Individual nanoplate subjected to continuous irradiation only and (i) its PL spectrum.

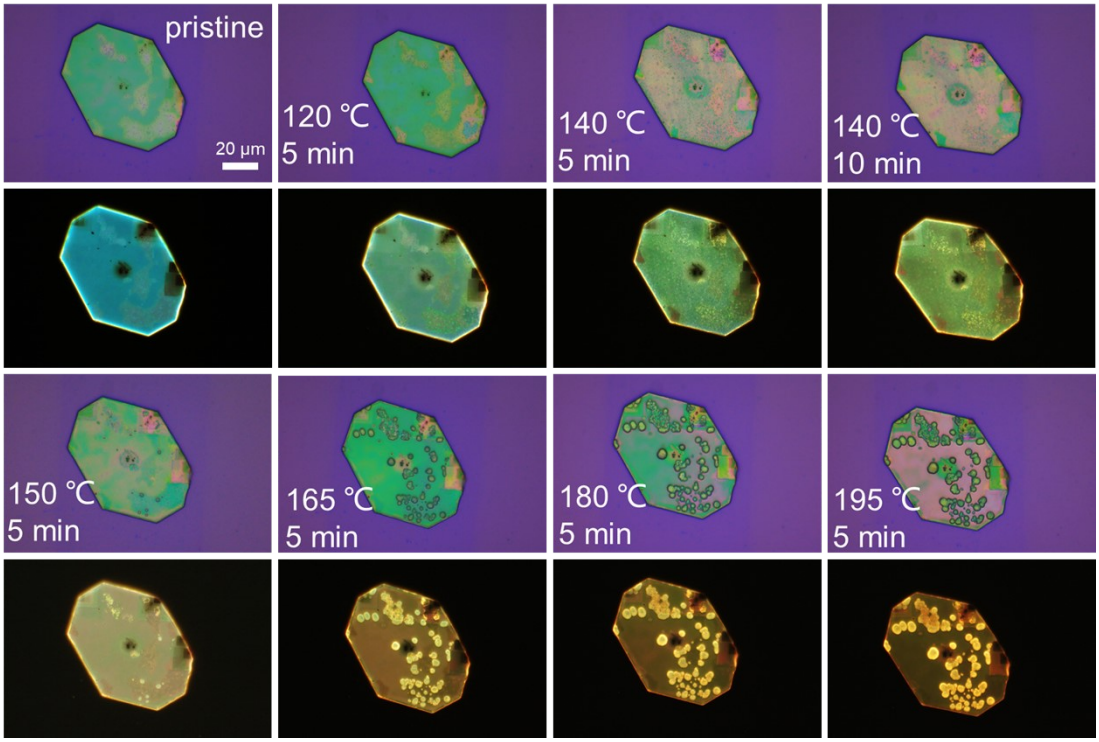

Fig. S11. OM and PL images of the nanoplates after the stepwise heating experiments.

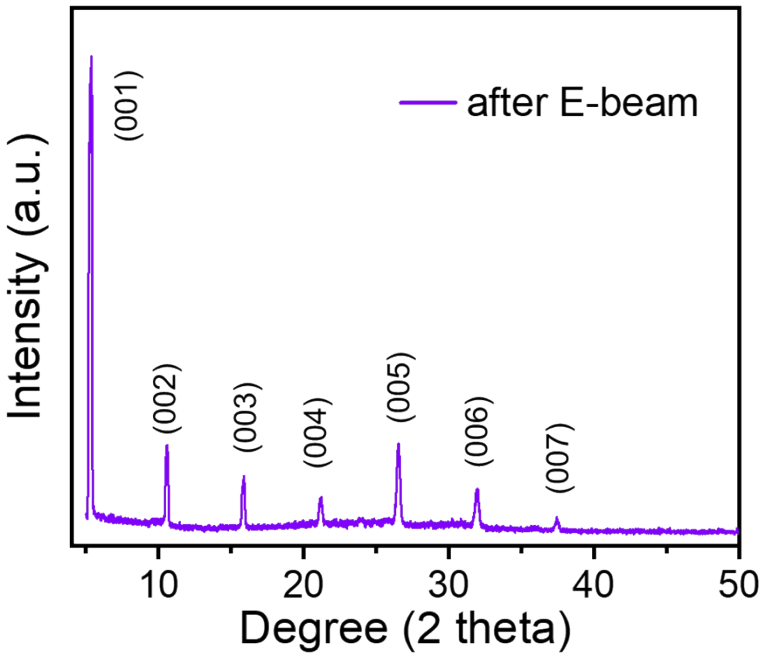

Fig. S12. XRD image of the PEA_2PbBr_4 nanosheets after radiation.

Table S1. XRD data of as-synthesized PEA_2PbBr_4 nanoplates

Lattice	001	002	003	004	005	006	007	008	009	0010	0011	0012
Peaks	5.39	10.71	16.05	21.38	26.80	32.27	37.82	43.48	49.22	55.11	61.17	67.42
FWHM	0.044	0.068	0.081	0.093	0.11	0.13	0.15	0.16	0.16	0.092	0.093	0.095
Δ_a	5.32	5.34	5.33	5.42	5.47	5.55	5.66	5.74	5.89	6.06	6.25	--

Δ_a represents the peak difference between adjacent crystal planes.

Table S2. XRD data after electron beam irradiation

Lattice	001	002	003	004	005	006	007
Peaks	5.35	10.60	15.87	21.21	26.53	31.95	37.42
FWHM	0.23	0.21	0.21	0.24	0.27	0.29	0.30
Δ_a	5.25	5.27	5.34	5.32	5.42	5.47	--
$\Delta_{(00n)}$	0.04	0.11	0.18	0.17	0.27	0.32	0.40

$\Delta_{(00n)}$ represents the peak difference on the same crystal plane before and after irradiation.

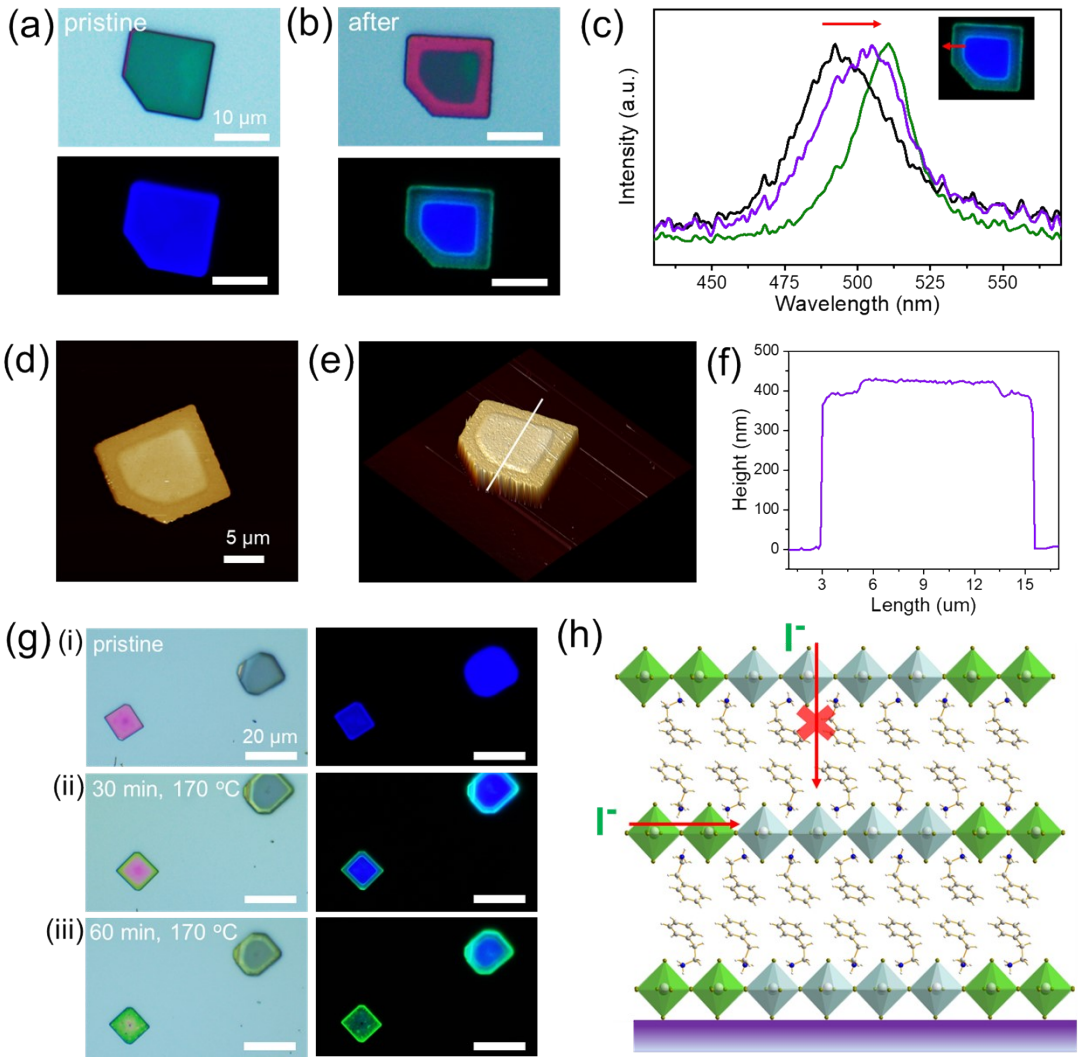

Fig. S13. OM and corresponding PL images of a nanoplate before (a) and after (b) anion exchange. (c) PL spectrum of the exchange region. (d) 2D AFM image after anion exchange. (e) Three-dimensional AFM image and (f) corresponding thickness profile after anion exchange. (g) OM and corresponding PL images: (i) Pristine sample. (ii) After annealing at 170 °C for 30 min. (iii) After further annealing at 170 °C for an additional 30 min. (h) Schematic illustration of anion exchange in PEA_2PbBr_4 nanoplates.

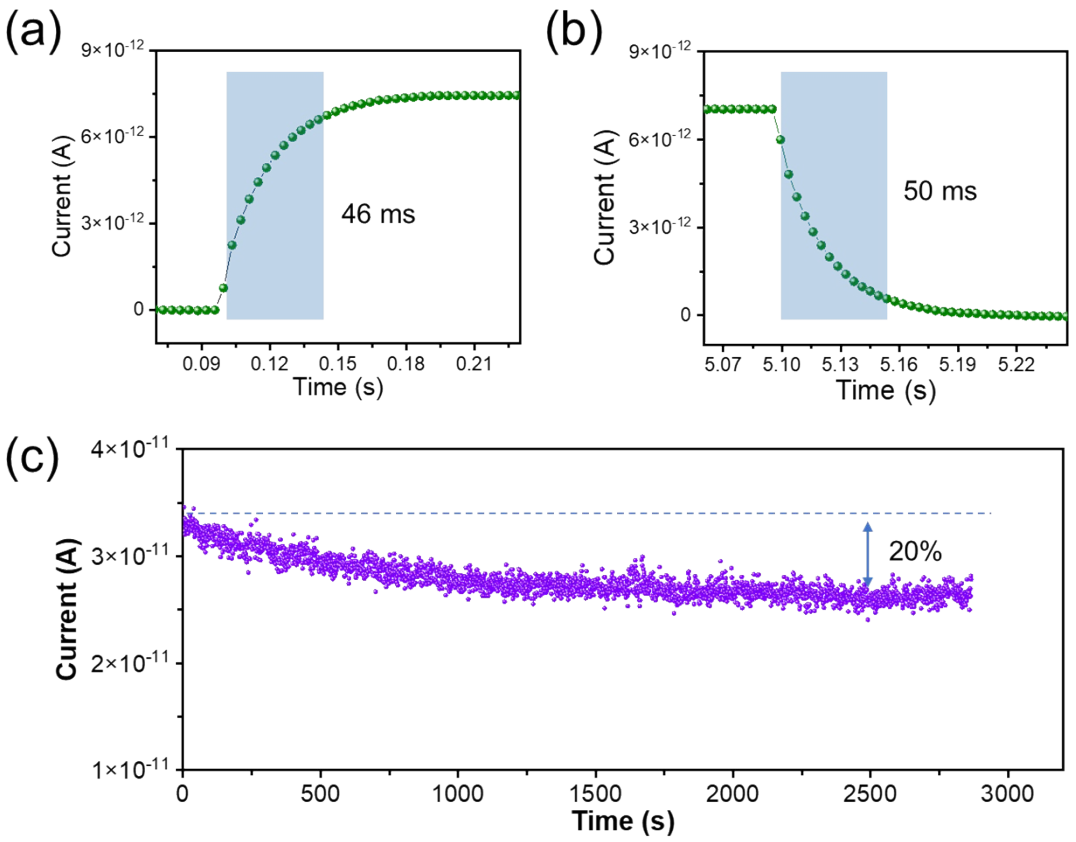

Fig. S14. Rise (a) and decay (b) time of PEA_2PbBr_4 nano-PD under 405 nm-UV light illumination. (c) Photocurrent of the device under continuous illumination at 1.1 mW/cm^2.

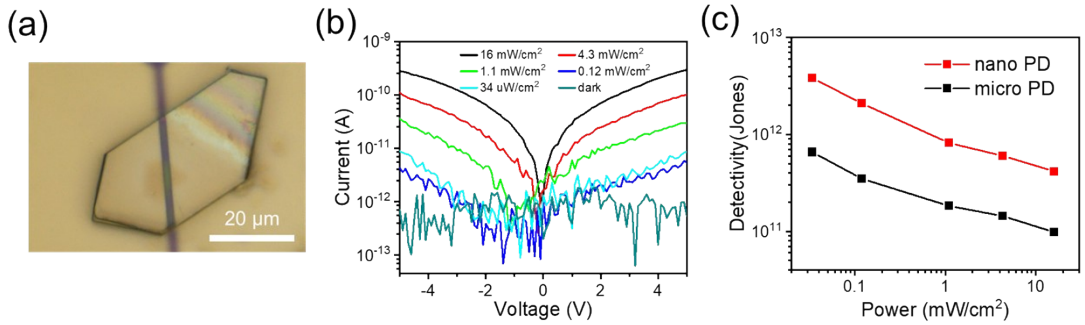

Fig. S15. (a) The micro-PD OM image. (b) I-V characteristics of PEA_2PbBr_4 micro-PD under various intensities of 405 nm light illumination and dark conditions. (c) The detectivity comparison between nano- and micro-PD.

Table S3. Comparison of the device performance parameters of 2D Br-based perovskite PDs reported in previous studies and this work.

Perovskite	Morphology	Laser (nm)	Intensity (uW/cm^2)	Bias (V)	Responsivity (A/W)	Detectivity (Jones)	Ref.
PEA_2PbBr_4	Nanoplate arrays	365	0.02	20	31.1	4.03×10^{13}	[1]
PA_2PbBr_4	Nanoplate	405	0.005	4	2.22	2.3×10^{13}	[2]
PA_2PbBr_4	Bulk	405	0.02	10	0.0912	6.08×10^{12}	[3]
BA_2PbBr_4	Bulk	377	0.08	10	0.0169	2.06×10^{12}	[4]
BA_2PbBr_4	Bulk	447	150	4	2.22×10^{-6}	2.99×10^{8}	[5]
$BA_2CsPb_2Br_7$	Bulk	377	0.48	10	8.55×10^{-3}	5.08×10^{11}	[6]
$BA_2CsPb_2Br_7$	Bulk	405	0.04	10	0.0395	1.7×10^{12}	[6]
BA_2PbBr_4	Bulk	400	2750	5	0.0453	1.08×10^{12}	[7]
PEA_2PbBr_4	Microplate	380	0.2	10	8.26×10^{-3}	1×10^{12}	[8]
$TRA_2CsPb_2Br_7$	Bulk	405	250	10	1.42×10^{-3}	7.45×10^{10}	[9]
PEA_2PbBr_4	Bulk	365	3	10	0.0315	1.55×10^{13}	[10]
$BA_2FAPb_2Br_7$	Bulk	405	0.082	1	5.1×10^{-4}	1.47×10^{13}	[11]
PEA_2PbBr_4	Nanoplate	405	0.003	5	1.6×10^{6}	1.1×10^{16}	[12]
PEA_2PbBr_4	Nanoplate	405	34	5	1.44	3.82×10^{12}	**This work**
PEA_2PbBr_4	Microplate	405	34	5	0.47	6.57×10^{11}	**This work**

The electrode material: [2] is carbon; [4] and [6] are Ag; all other electrodes are Au.

References

1. Y. H. Lee, J. Y. Park, P. Niu, H. Yang, D. Sun, L. Huang, J. Mei and L. Dou, *ACS Nano.*, 2023, **17**, 13840-13850.
2. K. Dong, H. Zhou, Z. Gao, M. Xu, L. Zhang, S. Zhou, H. Cui, S. Wang, C. Tao, W. Ke, F. Yao and G. Fang, *Adv. Funct. Mater.*, 2023, **34**, 2306941-2306950.
3. C. Zhang, H. Xiao, Q. Guan, T. Zhu, L. Liang, R. Li, H. Ye, X. Niu and J. Luo, *J. Mater. Chem. C*, 2023, **11**, 5116-5122.
4. L. Liang, X. Niu, X. Zhang, Z. Wang, J. Wu and J. Luo, *Adv. Optical Mater.*, 2022, **10**, 2201342-2201349.
5. E. Choi, Y. Zhang, A. M. Soufiani, M. Lee, R. F. Webster, M. E. Pollard, P. J. Reece, W. Lee, J. Seidel, J. Lim, J.-H. Yun and J. S. Yun, *npj 2D Mater. Appl.*, 2022, **6**, 43.
6. X. Niu, L. Liang, X. Zhang, Z. Wang, T. Zhu, J. Wu, Q. Guan, L. Hua and J. Luo, *Mater. Chem. Front.*, 2022, **6**, 3598-3604.
7. J. Wang, Y. Liu, S. Han, Y. Ma, Y. Li, Z. Xu, J. Luo, M. Hong and Z. Sun, *Sci. Bull.*, 2021, **66**, 158-163.
8. S. Wang, Y. Chen, J. Yao, G. Zhao, L. Li and G. Zou, *J. Mater. Chem. C*, 2021, **9**, 6498-6506.
9. F. Lédée, A. Ciavatti, M. Verdi, L. Basiricò and B. Fraboni, *Adv. Optical Mater.*, 2021, **10**, 2101145-2101154.
10. Y. Liu, J. Wang, S. Han, X. Liu, M. Li, Z. Xu, W. Guo, M. Hong, J. Luo and Z. Sun, *Chem. Eur. J.* , 2020, **26**, 3494-3498.
11. Y. Zhang, Y. Liu, Z. Xu, H. Ye, Q. Li, M. Hu, Z. Yang and S. Liu, *J. Mater. Chem. C*, 2019, **7**, 1584-1591.
12. Y. H. Lee, W. J. Lee, G. S. Lee, J. Y. Park, B. Yuan, Y. Won, J. Mun, H. Yang, S. D. Baek, H. Lee, J. H. Oh, T. J. Pennycook, G. Kim, J. Mei and L. Dou, *Adv. Mater.*, 2025, **37**, 2417761-2417772.